ACS NANO

www.acsnano.org

Jellyfish-Inspired Visual and Sensory Bubbling Robots with Automatic 3D Morphable Films for Underwater Environmental Interactions

Shan Li, Peng Xiao,* Qiling Wang, Jiang He, Xinrui Liu, Junjie Wei,* Yaowen Wang, and Tao Chen*

Cite This: *ACS Nano* 2024, 18, 20694−20705

ABSTRACT: **Coelenterates, such as Atolla jellyfish, are capable of integrating color, communication, and motion in a sophisticated manner, thereby enabling them to function as intelligent biological systems that can adapt to the challenges of the underwater environment. Extensive efforts have been dedicated to exploiting underwater visual, sensory, actuating, or combined systems. However, current biomimetic soft systems are still limited by the lack of comprehensive, integrated functional skins that can automatically deform, dynamically sense, and further send color signals when diving into underwater conditions. Here, we propose the synthetic soft skins composed of assembled entangled carbon nanotube networks and fluorescent unit-embedded elastomers which can be applied in a suspended form to allow autonomic 3D deformation, real-time perception, and dynamic fluorescence color transformation. The capabilities of the sensory and color display thresholds were controlled through the entanglement density of carbon nanotubes and the suspended area. As a demonstration, the soft thin skin was integrated into an artificial jellyfish robot, enabling the realization of a closed-loop feedback system for dynamic sensory processing, signal processing, and further 3D morphing-induced fluorescent color change, demonstrating significant potentials in underwater visual display, danger warning, and environmental exploration.**

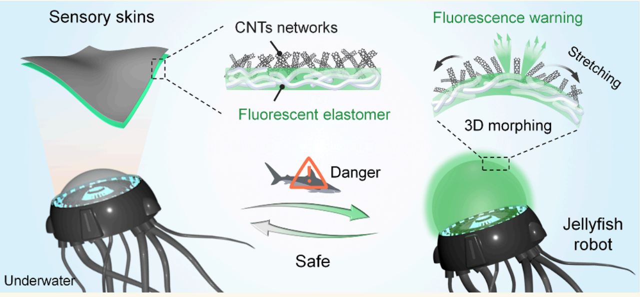

KEYWORDS: *soft skins, autonomous 3D morphing, self-perception, fluorescence warning, underwater environmental interaction*

1. INTRODUCTION

Biological systems show the capabilities to dynamically control their morphing, color, and shape,[1−4] enabling the realization of communications, camouflage, self-protection, and warning for surviving in harsh and varied environments.[5−7] An interesting organism of coelenterate Atolla jellyfish, coupled with stretchable skin and color-regulating organs, is capable of changing posture and color.[8−12] In artificial systems, the emerging biomimetic design of color-responsive soft actuators,[13−17] electronic skins,[18−23] and pneumatic/hydraulically driven environmental interaction systems (e.g., anticounterfeit and visual communication),[24−26] imitates creature-like sensory or motion behaviors, aiming to enrich the functions of certain machines, such as soft robots or artificial limbs.

Typical soft materials of silicon-based elastomers are widely applied to construct biomimetic soft robots to simulate two-dimensional (2D) or three-dimensional (3D) deformation of natural creatures due to their inherent flexibility, stretchability, and shape capability.[27−34] For example, Whitesides and co-workers[6] developed a soft quadruped robot with multicolor and patterned microfluidic network to realize discoloration and camouflage in visible and infrared light conditions. To introduce the sensory function, Chen and co-workers[35] and Sun and co-workers[36] presented a path to obtain flexible electronic skin with reversible mechanochromisms via strain-dependent cracks and folds. To combine these functions together, Shepherd and co-workers[16] demonstrated multi-layered electroluminescent skin-integrated soft actuators that enabled dynamic color-changing and sensory feedback via pneumatic actuation.

Despite the utilization of elastomers-based actuating or perception systems that enable skin-like motion and sensory behaviors, few soft actuators can integrate color, sensory, and morphing features into one skin.[14,19,37−40] In addition, current

Received: May 20, 2024
Revised: July 15, 2024
Accepted: July 19, 2024
Published: July 25, 2024

https://doi.org/10.1021/acsnano.4c06714
ACS Nano 2024, 18, 20694−20705

Scheme 1. **Illustration of Jellyfish-Inspired Visual and Sensory Bubbling Robots with Automatic 3D Morphable Films for Underwater Environmental Interactions**[a]

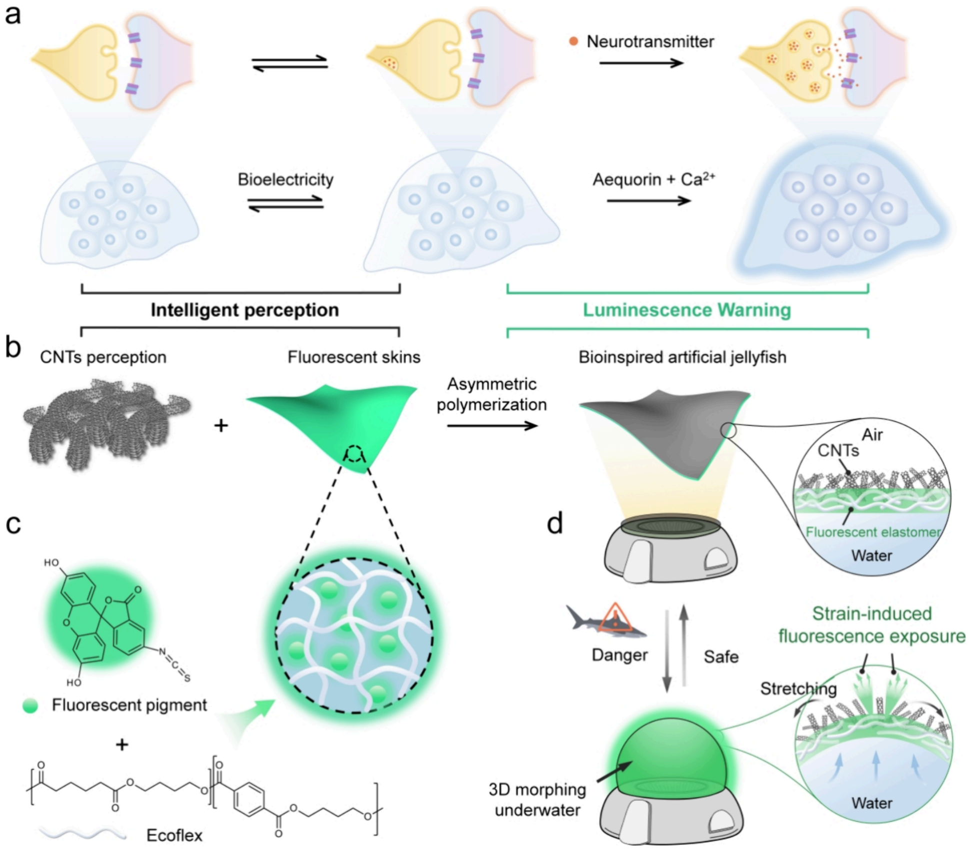

[a](a) Illustration showing Atolla jellyfish secreting neurotransmitters in response to bioelectrical stimulation, promoting the combination of aequorin and calcium ions for luminescence warning and communication. (b) Scheme of fabricating the bioinspired sensory, fluorescent, and morphable ultrathin films. (c) Schemes illustrating the structure of the designed fluorescent elastomer, which consisted of fluorescent pigments and cross-linked PDMS. (d) Schemes of warning mechanism for the artificial jellyfish robot. As the water depth increases, the integrated jellyfish robot exhibits 3D morphing resulting from the imbalance of internal air pressure and external water pressure. The illustration suggests that owing to the 3D deformation of the fluorescent thin skins, the CNT network on the surface is pulled apart, resulting in the underlying fluorescence being exposed.

single or integrated systems are usually applied in air conditioners. When they are exposed to a harsh underwater environment, some factors of high pressure, water wettability, and also fluid fluctuations could severely threaten the conductivity stability and controllable deformation capability.[41,42] To support the integrated functions in extreme water conditions, specific structural design and working mechanisms should be developed, which can help in the exploration of biological tracking and the underwater environment.

When Atolla jellyfish are subjected to an external stimulus, they emit a bright luminescence spontaneously through the combination of aequorin and calcium ions. This process serves to achieve self-protection and underwater communication[43,44] (Scheme 1a). Herein, inspired by jellyfish, we present an ultrathin and structurally integrated soft skin that enables autonomic underwater 3D morphing, sensitive perception, and also color display. The integrated actuators are composed of an entangled CNT network that is partially embedded into the ultrathin fluorescence doped elastomer, which is constructed on the water surface to achieve a thin and uniform membrane (CNT/fluorescence elastomer membrane, CFEM) (Scheme 1b, c). Superior to the rigid substrate, the interfacial reaction behaviors based on the air−water interface could be easily manipulated, transferred, and scaled up. In addition, unlike the conventional pneumatic or hydraulic actuators driven by an external pump, the skin-integrated underwater actuators can experience autonomic 3D morphing when diving into water. The 3D deformation of the actuator results in a homogeneous strain of the entangled CNT network and exposure of doped fluorescent molecules, which can achieve dynamic electrical signals and reversible mechanochromism display via strain-dependent microcracks effect. As a demonstration, a soft actuator-based artificial jellyfish robot close-loop system is designed. It can sensitively perceive the intensity of water vibration and further transport the signals and analyze the predesigned warning threshold via the microprocessor. Over the intensity threshold, the robot dives and further experiences an autonomic 3D morphing and fluorescence display for danger warning (Scheme 1d).

2. RESULTS AND DISCUSSION

2.1. Fabrication and Fluorescence Properties of CFEM. To construct elastic and conductive biomimetic soft skins, a fabrication strategy based on liquid substrate is achieved in Figure 1a. A compact and stable CNT film can be obtained through a typical self-assembly strategy on the water

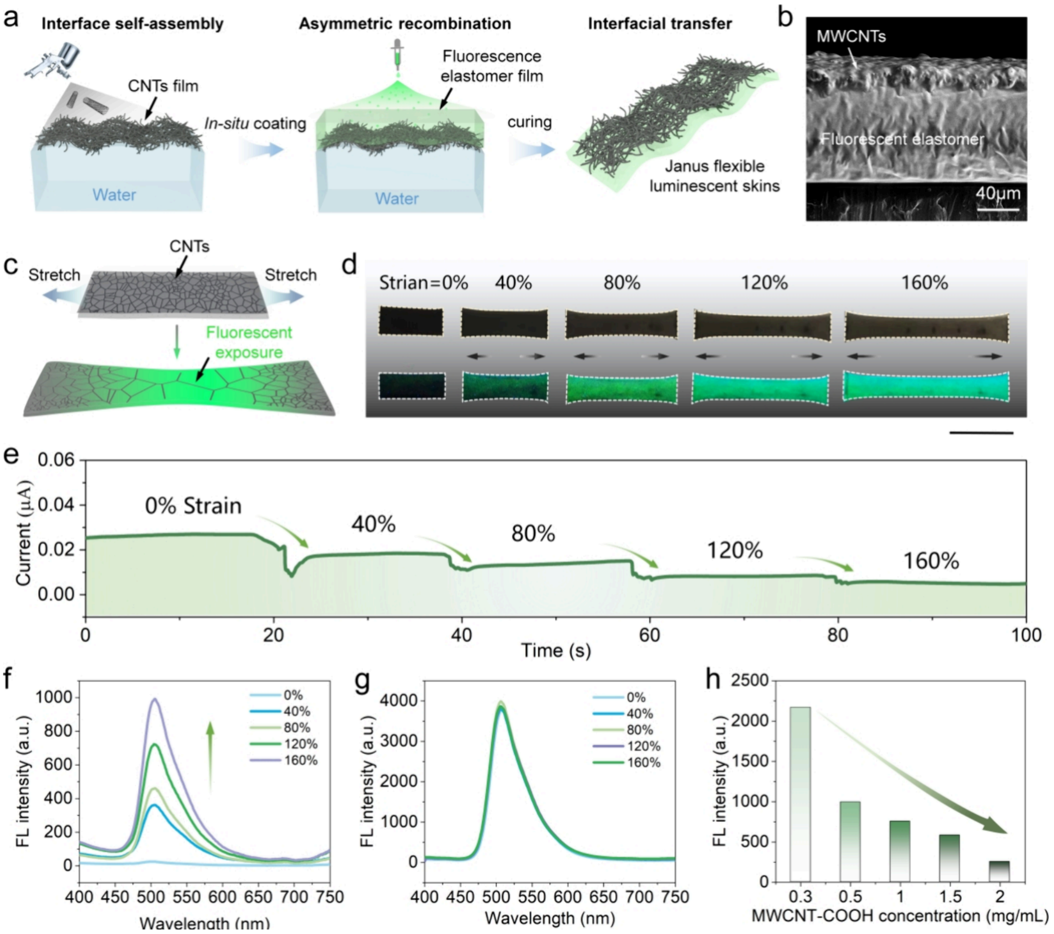

Figure 1. Fabrication and fluorescence property of CFEM. (a) Schematic diagram of preparation for CFEM-based fluorescent skins. In detail, it includes the self-assembly of CNTs film based on Marangoni effect at water/air surface and asymmetric functionalization of Ecoflex mixed with fluorochrome. (b) Cross-sectional SEM image of the CFEM. Schematic diagram of CFEM uniaxial stretching with fluorescent exposure (c) and UV images under different strains (0, 40, 80, 120, and 160%) (d) (scale bar: 2 cm). (e) Current versus time curves of CFEM. The fluorescence curves of CFEM with CNT concentrations of 0 mg/mL (f) and 0.5 mg/mL (g). (h) Fluorescence intensities of CFEM with different CNT concentrations under 160% strain.

surface enabled by the Marangoni effect and the capillary force driving compression. Based on the interface functionalization strategy,[45] the water-supported CNT film can be further functionalized by fluorescent elastomer via in situ composite to achieve the fluorescent and conductive film, among which the CNT network was partially embedded into an elastic matrix with satisfactory structural stability. Digital images of the CNT film and asymmetric composite fluorescent skins at the water/air interface are displayed in Figure S1. Apparently, CNT films can be readily obtained via interface self-assembly, and the in situ composited CFEM presents a slight green color. Compared with CFEM covered with a CNT network, the elastomer without a CNT network emits green fluorescence under the irradiation of a 254 nm ultraviolet lamp. SEM images of the CNT side and elastomer side of the CFEM are shown in Figure S2. It can be observed clearly that at the water side of the Janus film, CNTs stretch out of the Ecoflex and ensure the conductive pathways, while the elastomer side shows a wrinkled surface. This result can be attributed to the immiscibility between Ecoflex/N-hexane and water. In order to prove the reliability of the surface composite method, the mechanical properties of the pure CNT film and CFEM were further explored (Figure S3). It can be observed that the CNT film is weakly bound to the glass plates, while the CNTs are stably interlocked in the polymer network. Moreover, the asymmetric structure can be further supported by the water contact angle (WCA) on both sides of the CFEM. As shown in Figure S4, the WCA on the CNT side increased from 21 ± 1.4 to 111.6 ± 0.9° after composited, while the WCA on the Ecoflex side did not change significantly (~109.7°), indicating that CNTs were successfully embedded in one side of the Ecoflex matrix. The cross-sectional structure of CFEM was also characterized, which showed an obvious asymmetric design and good combinative ability between two layers (Figure 1b).

The fluorescence performance of CFEM was quantified by means of a uniaxial tension test under strain ranging from 0 to 160% (Figure 1c,d). It was noticeable that with the increase of uniaxial strain, the colors of CFEM changed from dark to bright green, indicating that the fluorescent skins possessed a significantly strain-dependent fluorescence responsive behavior. In the process, randomly entangled nanotubes fixed in the elastic polymer were gradually stretched, and the corresponding conductive paths were disconnected, leading to a decreased tendency in current (Figure 1e). The real-time fluorescence display and the stress-time curve of CFEM under uniaxial tension are presented in Movie S1 and Figure S5, respectively, showing a positive correlation between strain and fluorescence intensity. Polarizing microscope images of CFEM under

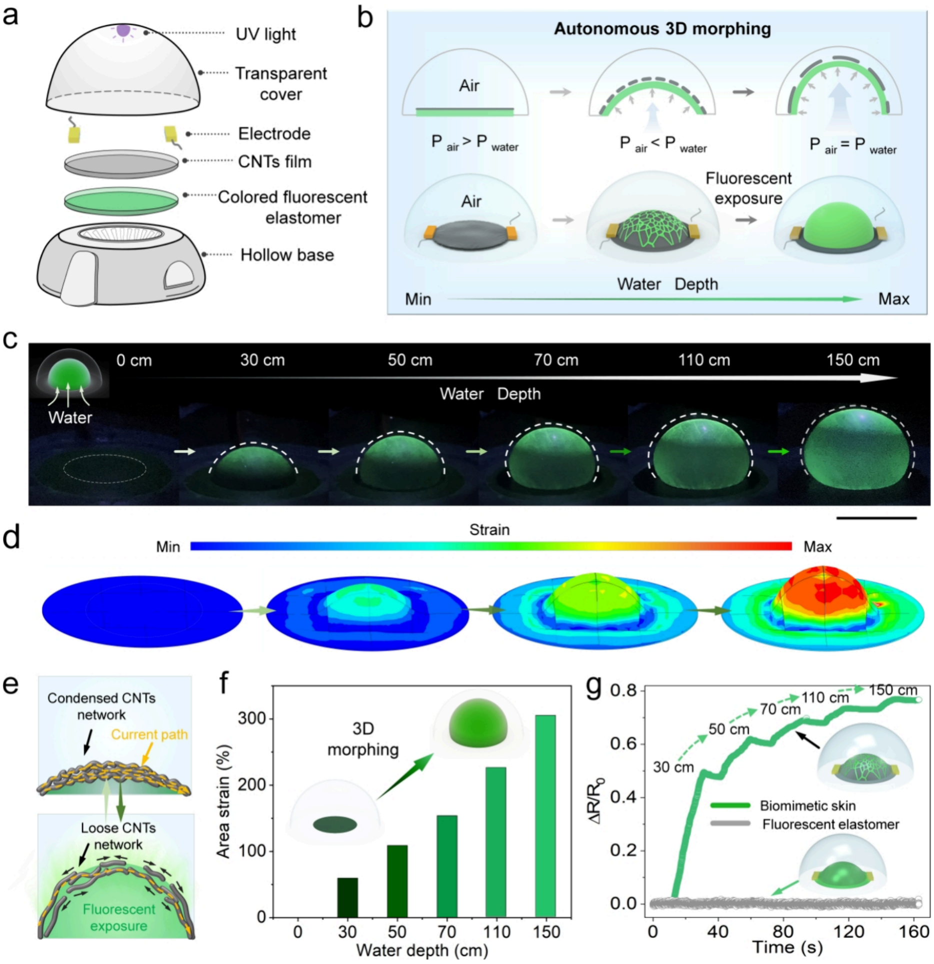

Figure 2. Structural design and working mechanism of the CFEM jellyfish robot. (a) Schematic diagram of split structures of the jellyfish robot. (b) Mechanism diagram of 3D morphing-induced fluorescence of the CFEM jellyfish robot as the water depth increases. (c) Fluorescence photographs of the prepared jellyfish robot with 3D morphing at 0, 30, 50, 70, 110, and 150 cm underwater (scale bar: 20 mm). (d) Abaqus simulation of the 3D deformation process of the CFEM jellyfish robot. (e) Fluorescent mechanism diagram of CFEM. (f) Area strain curve of the CFEM under corresponding water depths. (g) Normalized resistance versus curve of fluorescent elastomers with or without CNT layer under water depths of 0, 30, 50, 70, 110, and 150 cm.

different strains also supported the conclusion (Figure S6). Moreover, the TEM images of unentangled multi-walled carbon nanotubes show a curved and flexible morphology, which is conducive to the dynamic display of fluorescence (Figure S7). The microcracks under different tensile strains are shown in Figure S8. It is evident that with the increase of tensile displacement, the microcrack size extends continuously. The CNTs network, which is embedded on one side of the CFEM, not only assists in effective fluorescence display but also enables water depth monitoring through its intrinsic conductivity. We further investigated the fluorescence intensities of CFEM with the CNT concentrations of 0, 0.3, 0.5, 1.0, 1.5, and 2.0 mg/mL, respectively (Figure S9). When CFEM is excited by 254 nm UV light, the emission wavelength of green fluorescence is ~506 nm. Compared with the pure fluorescent elastomer, the green fluorescence intensities of CFEM exhibit a positive correlation with tensile strain, while the fluorescence intensity of the pure fluorescent elastomer remains unchanged (Figure 1f, g). Owing to the stable baseline of the fluorescence spectrum (strain = 0%) at 0.5 mg/mL CNT concentration, it is selected as the best display sample for objects, fluorescence images, and current in our work. More importantly, it was found that with the increase of CNT concentration, the fluorescence intensity of CFEM under 160% strain presented a decreasing tendency (Figure 1h). The covered fluorescence is difficult to transmit as a result of the thicker CNT film per unit area.

2.2. Structural Design and Mechanism of CFEM-Based Artificial Jellyfish. The robot designed with a jellyfish-like structure is assembled from UV light, electrode, CNTs film, fluorescent elastomer, transparent cover, and hollow base (Figure 2a). Owing to the flexibility and thinness of the fluorescent skins, the prepared CFEM can be easily transferred onto a substrate with a hollow ring. When a steel sperm was applied to the self-supported flexible membrane, CFEM can exhibit significant strain and clearly reproduce fingerprints (Figure S10). The diameter of the fluorescent skins can be self-edited via laser cutting, and the transparent cover can be sealed by Ecoflex prepolymer. As the water depth increased, an interesting competitive relationship was shown in external hydraulic pressure and internal air pressure, resulting in CFEM fluorescence display behavior (Figure 2b). In shallow water, the assembled skins of the CFEM jellyfish robot exhibit no deformation. As the water depth increased, the enhanced water pressure caused the fluorescent skins to display 3D morphing. Subsequently, the CNT network on the CFEM surface is stretched, which induces the generation of microcracks following the green fluorescence exposure. Moreover, the asymmetric structure of CFEM not only enables the controlled fluorescence display but also protects the intrinsic mechanical properties of the elastomer. Similar to the pure Ecoflex film, the composite CFEM exhibits high flexibility (1288 kPa) and strain capacity (496%), which ensures the successful implementation of 3D morphing (Figure S11). Fluorescence photographs of the CFEM jellyfish robot under different water depths are presented in Figure 2c. The CFEM jellyfish robot swam from the water depth of 0 to 150 cm, and the CFEM gradually expanded autonomously in a hemispherical shape (Figure S12), resulting in the stretching of the CNT network. As a result, the CFEM jellyfish robot can display green fluorescence of different intensities under different water depths. The process operates without human intervention or large equipment and the CFEM jellyfish robot can spontaneously experience 3D morphing as the water depth increases.

Additionally, finite element simulation and analysis enabled by the Abaqus software were also conducted to simulate the strain distribution of the CFEM jellyfish robot under the generated 3D strain (Figure 2d). It is evident that the greatest strain distribution occurs at the top of the 3D morphing, where the CNT network is sufficiently stretched and the green fluorescence is most exposed. The results are consistent with the real-time fluorescence images shown in Figure 2c. In our work, a simplified sketch of a potential fluorescent mechanism is schematically illustrated in Figure 2e. With the increase of 3D morphing, randomly entangled nanotubes fixed in the elastic polymer experience rapid displacement and cause larger cracks generation; thus, the transmission of the CNT layer is increased and the deformed CFEM emits green fluorescence through the gaps. Meanwhile, the conductive pathways caused by stretched CNT networks are decreased, resulting in an obvious resistance change. This mechanism demonstrates that the CFEM jellyfish robot can achieve depth perception beyond that of the biological jellyfish. The real area strains of the CFEM jellyfish robot under different water depths can be calculated by the surface area formula of the spherical crown, as shown in eq 1:

$$S = \int_{\theta}^{\pi/2} 2\pi rR\cdot \mathrm{d}\theta = 2\pi RH \tag{1}$$

where R and H are the radius of the 3D sphere and the height of the crown, respectively. The 3D deformation of the CFEM jellyfish robot can be approximated as being part of a sphere. It can be clearly observed that the area strains increase significantly from 0 to 305% as the water depth increases from 0 to 150 cm (Figure 2f). Moreover, the real-time resistance response corresponding to water depths can be easily monitored by the CFEM jellyfish robot. As displayed in Figure 2g, when the CFEM jellyfish robot was at 0, 30, 50, 70, 110, and 150 cm underwater, the normalized resistance represented an increased tendency with the ladder pattern. In contrast, pure fluorescent elastomers without CNT network demonstrated a constant resistance value at any water depth. We further calculated the forces on the artificial jellyfish robot under different water depths (Figure S13). The underwater force of the jellyfish robot was positively correlated with water depth, and compared with the uniaxial tensile force, the force at deep water is greater than the uniaxial stress.

2.3. Editability of the CFEM Jellyfish Robot in Time/Space Dimension.

Based on the above results, the CFEM can be further inflated to realize a stretch for 3D displacement with the help of a self-supported device. The shade and bright fluorescence of the CFEM jellyfish robot can be achieved via the resulting 2D to 3D transformation, which is similar to the display strategy of organisms (e.g., warning luminescence of jellyfish). Superior to the conventional 2D deformation system, the introduction of fluorescence and sensing functions into the 3D system is conducive to direct and accurate 3D image camouflage and information exchange behavior. Therefore, the barometric actuator based on CFEM was also constructed to adjust the CNT concentration for designing fluorescence responses in different time dimensions. When the air pressure increased from 0 to 280 Pa, a 2D self-supported CFEM developed into a 3D hemispherical structure, resulting in cracks generation and gradual green fluorescent display (Figure S14). We further explored the 3D fluorescence display behaviors of CFEM (diameter = 40 mm) with CNT concentrations of 0.3, 1.0, and 2.0 mg/mL. It can be clearly observed that the lower the concentration of CNTs, the earlier green fluorescent exposure completely, indicating that the concentration of CNTs can effectively adjust the time sequence of full fluorescent exposure. The area strain of 3D morphing gradually increases from 0 to 74.71% as the pressure increases (Figure S15), and this process can be effectively monitored via dynamic stretched CNT networks (Figure S16). Moreover, the normalized resistance-strain curves under different CNT concentrations of 3D-based CFEM were investigated. It can be found that when a higher content of CNT was applied, the gauge factors (GF) showed a decrease at high strain. The results can be attributed to the smaller relative displacement of the high-concentration CNT network (Figure S17). Note that a higher concentration (>2 mg mL^{-1}) could not be applied in our experiment owing to the poor dispersion of CNTs in ethanol solvent.

In addition to luminous brightness, it is greatly significant to explore the maximum diving depth of the CFEM jellyfish robot, which can facilitate us to further understand the differences in the underwater environment and creatures at different water depths.[46] The CFEM jellyfish robots with diameters of 10, 20, and 30 mm are driven from 0 cm to 110, 120, and 160 cm, respectively, underwater, and sectional area strains of different diameters are displayed in Figure S18. With the increase in driving depth, the CFEM jellyfish robot with a smaller diameter shows greater strain and an almost spherical structure. The normalized resistance curves of the diving depth in a gradient of 10 cm were monitored in Figure S19 and the artificial jellyfish robot enables the perception of the underwater position. With the increase of diameter from 10 to 30 mm, the maximum diving depth of the CFEM jellyfish robot has been increased from 120 to 190 cm underwater. As a result, there is a positive relation between the diameter and the maximum diving depth of the designed jellyfish robot. Note that upon continuously driving into the deeper water, the CFEM jellyfish robot will burst under water pressure. CFEM still has good stability in solutions with acid, alkali, and seawater salt concentrations, and the surface morphology is not corroded (Figure S20). More importantly, the CFEM-based robot shows excellent long-term electrical stability, durability, and reliability for tracking the repeatedly diving processes (Figure S21). In conclusion, the fluorescence display time and the maximum reached water depths of the CFEM jellyfish

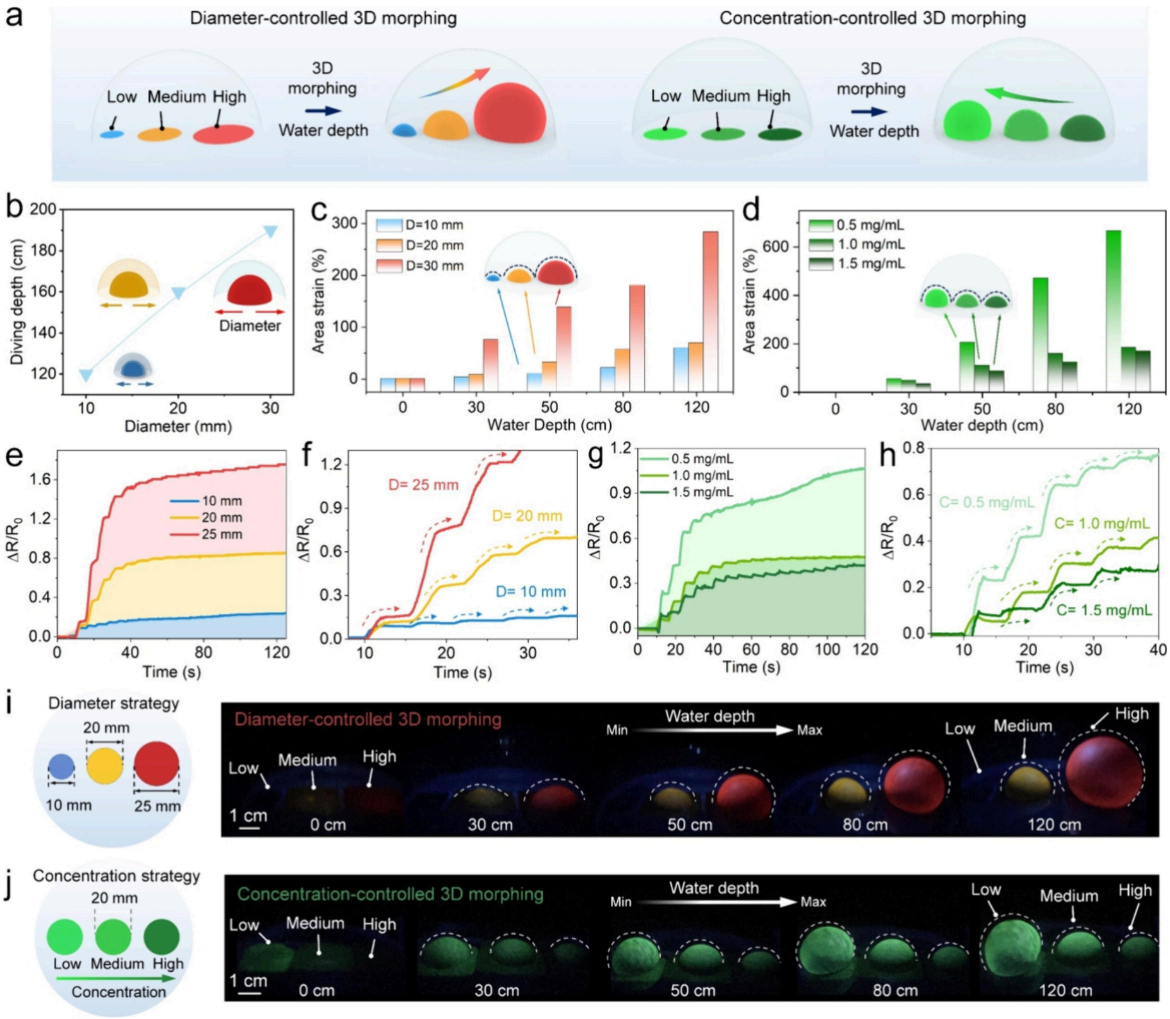

Figure 3. Multicolor edited and integrated CFEM-based artificial jellyfish. (a) 3D morphing diagrams of diameter and concentration-controlled in integrated CFEM jellyfish robot underwater. (b) Maximum driving water depths of the individual CFEM jellyfish robot at different diameters. (c, d) Area strain versus of the CFEM jellyfish robots featured with multicolor and gradient color under water depths in 0, 30, 50, 80, and 120 cm. (e) Resistance versus time curves of the integrated CFEM jellyfish robot with three different diameters (10, 20, and 25 mm) driving underwater. (f) Resistance variation tendency at low water depths of the diameter-designed CFEM jellyfish robot. (g) The resistance curves of driving underwater of the integrated CFEM jellyfish robot with CNT concentrations of 0.5, 1.0, 1.5 mg/mL. (h) Resistance increasing tendency at low water depths of the concentration-designed CFEM jellyfish robot. (i) Multicolor fluorescence display diagrams and photographs of the diameter-edited jellyfish robot (10, 20, and 30 mm) under increasing water depths. (j) Gradient fluorescence photographs of the concentration-edited (0.5, 1.0, and 1.5 mg/mL) jellyfish robot as water depths increase.

robot can be flexibly and effectively regulated by the concentration of CNT and the diameters of fluorescent skins.

2.4. Underwater Integrated Visual Display of the Artificial Jellyfish.

Natural organisms change their body color for the purpose of camouflage via stretchable skin and multiple morphing forms in extreme conditions.[26,47] The appropriate introduction of diverse colors into soft robots can facilitate information exchange and visual display between humans and machines, especially for underwater soft robots.[48,49] As a proof of concept, color, diameters, and CNT concentration were integrated into one system to achieve a 3D diversified display. As shown in Figure 3a, we explored the 3D actuation and fluorescent behaviors of the integrated jellyfish system with three diameters and three CNT concentrations, respectively. First, the diving depths of the single CFEM jellyfish robots with different diameters (10, 20, and 30 mm) were explored, which can eventually reach maximum water depths of 120, 160, and 190 cm, respectively (Figure 3b). Furthermore, the area strain of CFEM jellyfish robots featured with multicolor and gradient color can be effectively calculated in driving depths of 0, 30, 50, 80, and 120 cm (Figures S22 and 23). In the multicolor fluorescence system, 3D deformation is positively correlated with the designed diameter with the increase of water depths, which can be attributed to the deformation area (S) of the CFEM being positively correlated with the applied force (F), resulting in greater 3D deformation ($P = F/S$, P is a constant value under the specific water depth) (Figure 3c). The fluorescence curves of CFEM with yellow and red colors were also characterized in Figure S24, showing an increasing tendency with the strain increasing from 0 to 160%. The conclusions presented above are in accordance with the proposed mechanism of strain-dependent fluorescence exposure. Furthermore, the excitation wavelengths of CFEM with three fluorescence colors were investigated under the strain of 160% (Figure S25). It can be observed that the green and yellow fluorescent elastomers can also be excited in the

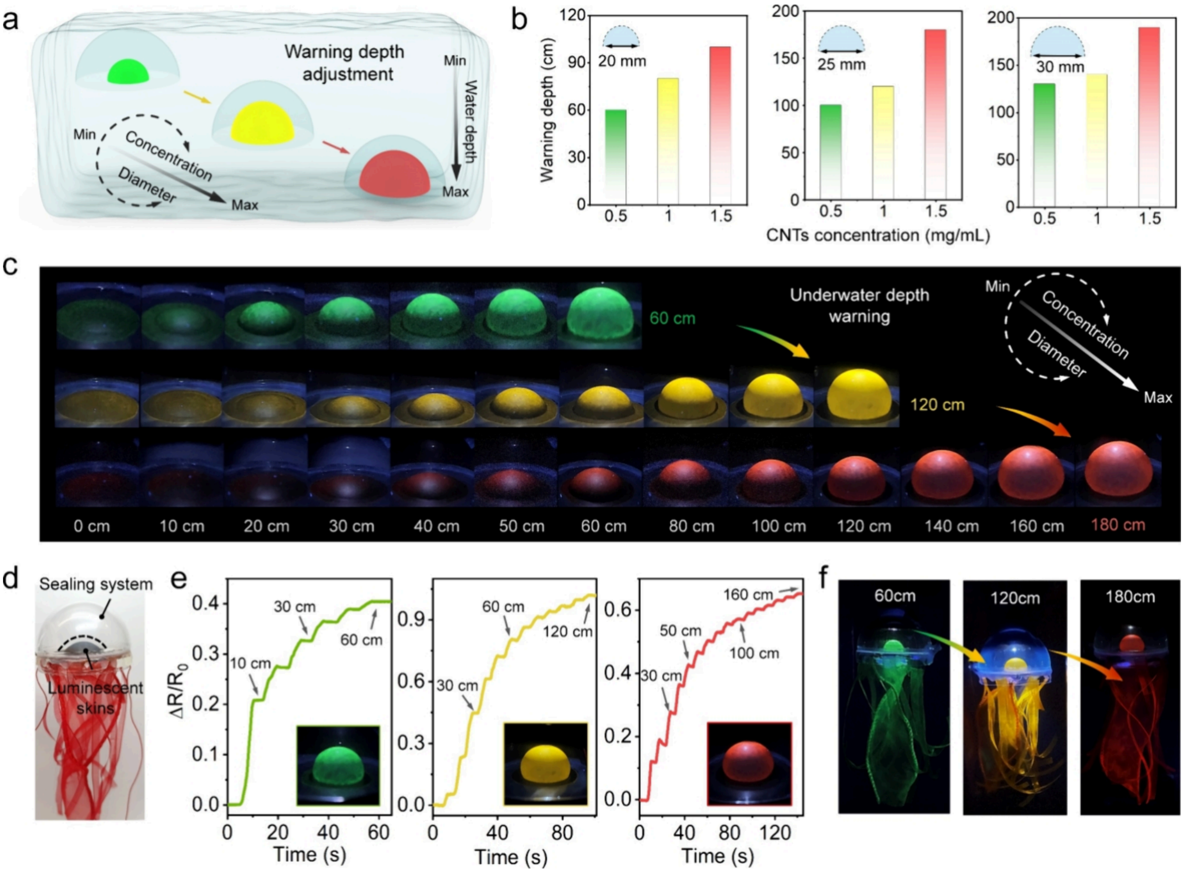

Figure 4. Underwater depth warning of CFEM-based artificial jellyfish. (a) Underwater depth warning diagram of the achieved fluorescent jellyfish robot via the combination of CNT concentration and diameter. (b) Maximum warning depth curves of the designed jellyfish robot under different diameters and concentrations. (c) Underwater depth warning photographs of the CFEM-based jellyfish robot for a series of controllable 3D deformation, introducing three fluorescent colors (green, yellow, and red) to warn different water depths (60, 120, and 180 cm). (d) Optical photograph of the CFEM-based jellyfish robot featured with 3D deformative and self-perceptive functions. (e) Real-time resistance versus time curves with a 10 cm gradient of the designed depth warning jellyfish robot underwater. (f) Underwater fluorescence images of the CFEM-based jellyfish robot at depths of 60, 120, and 180 cm, enabling a color mapping of depth warning.

visible region (~450 nm), while the excitation wavelength of the red fluorescence elastomers is mainly in the ultraviolet region. Therefore, ultraviolet light is applied as the excitation wavelength in order to achieve an underwater multicolor visual display. However, there is an opposite tendency in the gradient color system. With the increase in the CNT concentration, the area strain of the integrated jellyfish robot (20 mm) shows a decreasing tendency at the same water depth (Figure 3d). This may be because the high CNT concentration could have a greater effect on the intrinsic mechanical properties of elastomers (Figure S26).

To measure the properties of 3D morphing, a closed model with three little "jellyfish" was designed and further integrated with the CFEM and electrodes. When the integrated jellyfish robots experienced controllable actuation at an increasing driving depth with a gradient of 10 cm, the real-time normalized resistance time curves demonstrated the strain-strengthening effect in the multicolor CFEM jellyfish system as the diameter increased (Figure 3e). In order to clearly observe the electrical signal, an enlarged normalized resistance curve with three diameters is shown in Figure 3f, which is consistent with the 3D morphology in Figure 3c. Similarly, we also monitored the ladder-shaped electrical signal of the integrated jellyfish system with the same diameter and CNT concentrations of 0.5, 1.0, and 1.5 mg/mL respectively (Figure 3g,h). It can be found that compared with the other two, the little CFEM "jellyfish" of 0.5 mg/mL displays a greater relative resistance change and further confirms the enhanced 3D deformation, which is consistent with the area strain tendency in obtained Figure 2d. To observe the 3D shape-morphing behaviors, three different colors, blue, yellow, and red, were introduced into the integrated artificial jellyfish robot, corresponding to three little CFEM jellyfish with diameters of 10, 20, and 25 mm, respectively (Figure 3i). With the increase of water depth, 3D morphing of the red, yellow, and blue integrated jellyfish robots presents an increasing tendency. Furthermore, the hydraulic actuating process of the concentration-controlled CFEM-based jellyfish robot was effectively captured (Figure 3j). The CNT concentrations from low to high endowed the CFEM jellyfish robot with a gradient color. In this ingenious integrated system, diverse visual displays can be achieved through the design of concentration, color, and diameter of jellyfish, which can further provide an integrated platform underwater for self-regulated multicolor robot systems.

2.5. Underwater Depth Warning of the CFEM-Based Artificial Jellyfish. Natural organisms can adapt to underwater environments through training, but visualized acquisition of depth perception is challenging for avoiding danger.[50,51] In our work, we further developed a self-perceptive and

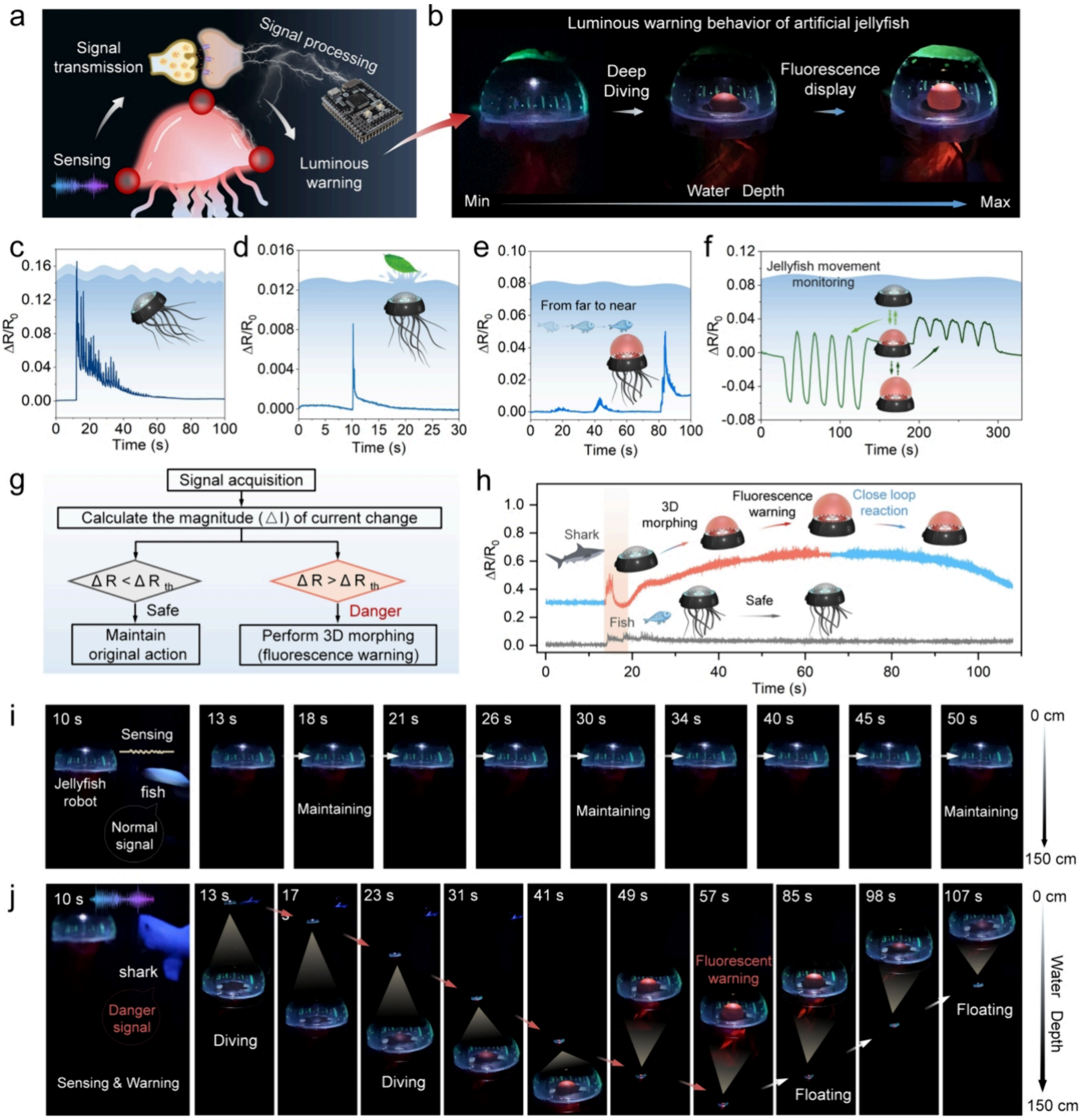

Figure 5. Bioinspired CFEM jellyfish robot for autonomous underwater environment interactive system. (a) Schematic illustration of a real jellyfish fluorescence warning, including sensing, signal transmission and processing, and warning. (b) Fluorescence warning behaviors underwater of the CFEM-based artificial jellyfish robot, showing a 3D morphing and red fluorescence displays. (c, d) Normalized resistance curve of the artificial jellyfish robot applied a wave and a falling object (0.96 g). (e) Normalized resistance curve of underwater disturbance signals from far and near. (f) Real-time resistance curve for the artificial jellyfish diving up and down underwater. (g) Working mechanism of underwater interaction system based on CFEM Jellyfish robot. (h) Normalized resistance time curves of the artificial jellyfish robot under external stimulus, showing a sharp improvement in danger conditions and maintaining a constant value in safe conditions. (i) Photographs of the CFEM-based jellyfish robot maintained a consistent water depth under normal signal stimulations. (j) Photographs of the CFEM-based jellyfish robot driving from 0 to 150 cm underwater at a constant speed of ∼3.41 cm/s for a series of controllable 3D deformation and fluorescent warning in a dangerous environment. The images in (i) and (j) are obtained from Movies S2 and S3, respectively.

fluorescent jellyfish robot to monitor and achieve fluorescence warning behavior with the increase of water depths. Warning depth adjustment of the developed jellyfish robot can be realized through the accurate combination of CNT concentration and diameter (Figure 4a). To prove the possibility of fluorescence warning of the 3D morphing jellyfish robot, we alternatively introduced three fluorescent pigments of green, yellow, and red colors into the CFEM-based robot to observe the fluorescence display at the maximum warning depth. The regulated jellyfish robots with three diameters of 20, 25, and 30 mm show the increasing warning depths at different CNT concentrations (0.5, 1.0, and 1.5 mg/mL), which is summarized in Figure 4b. When the 20 mm diameter was applied to the artificial jellyfish robot, the maximum fluorescence intensities appeared at water depths of 60, 80, and 100 cm as CNT concentration increased (Figures S27 and 28). These depths were considered to be the warning depths, and the 20 and 30 mm diameters were calculated in a similar manner.

Through an alternative combination of diameter and concentration, the designed CFEM artificial jellyfish can be endowed with the capability of depth warning underwater. We defined underwater as three parts: shallow zone (60 cm), buffer zone (120 cm), and deep zone (180 cm), which can be distinguished by fluorescent colors. As displayed in Figure 4c, the green fluorescent jellyfish robot with a 0.5 mg/mL concentration and 20 mm diameter can warn the water depths from 0 to 60 cm via 3D morphing-induced fluorescent display. Note that there is no significant change in fluorescence color above 60 cm underwater, and the designed artificial jellyfish will be irreversibly damaged. Moreover, the underwater warning depths of 120 and 180 cm were also investigated via the designed yellow and red fluorescent jellyfish robot. As a result, combined with concentration and diameter, the maximum depths under different water zones can be forewarned through different fluorescent color jellyfish. Optical photographs of the CFEM-based jellyfish robot featured with 3D deformation are achieved in Figure 4d. With the increase of water depths from 0 to 180 cm, the corresponding electrical signals of the CFEM-based jellyfish robot with depth warning can be captured accurately, which presents a step-by-step increase (Figure 4e). Moreover, underwater fluorescence images of the CFEM-based jellyfish robot at depths of 60, 120, and 180 cm are also displayed (Figure 4f). The active perception and underwater fluorescence display can provide an early warning to effectively respond to the dangers in the marine environment. For example, when someone dives into a deep zone, the CFEM jellyfish robot can emit bright red fluorescence or transmit an electrical signal to warn and alert people.

2.6. Bioinspired Artificial Jellyfish Robot for the Underwater Interactive System. In nature, jellyfish skins are endowed with capabilities of self-perception and desirable 3D deformation to adapt to the complex underwater environment. Importantly, when an external stimulus is applied to a jellyfish, the received signal from the jellyfish's skins can be transmitted and processed effectively and finally induce a luminous behavior to achieve active self-protection (Figure 5a). Inspired by the natural phenomenon, we demonstrate an autonomic 3D-deformative self-perceptive CFEM jellyfish robot that can achieve sensing and autonomous feedback (strain-induced fluorescence exposure) to avoid danger. In this process, the microprocessor and driving system are designed to imitate and operate the signal processing and 3D actuation of the artificial jellyfish, respectively. The fluorescent warning behavior of the obtained artificial jellyfish can be clearly observed in Figure 5b, which shows 3D deformation and red fluorescence display with the increase of water depth. Furthermore, the developed CFEM jellyfish robot possesses the ability to monitor signals both horizontally and vertically underwater. For instance, a typical red jellyfish robot can successfully monitor the surface frequency of the water (2, 0.8, and 0.4 Hz) by tapping the tank wall. Additionally, different water velocities can be detected separately by calculating the water column per unit area (Figure S29). The artificial jellyfish robot with ultrathin and structurally integrated soft skin can even show the ability to detect microsignals, such as waves and a falling object (Figure 5c,d), and also exhibit a rapid response time (~0.105 s) (Figure S30). In our system, the artificial jellyfish robot can even perceive disturbance signals from the surrounding environment at underwater depths of 20, 40, and 60 cm, which may provide ideas for underwater exploration (Figure S31). As a case, the CFEM-based jellyfish robot was placed at a water depth of 60 cm and was able to detect disturbance signals from both distant and nearby fish (Figure 5e). To mimic the swimming pattern of natural jellyfish, the artificial jellyfish robot performs diving up and down with a depth gradient of 30 cm. It can be clearly observed that the real-time electrical signal of the diving movement is consistent with the tendency of 3D morphing of the CFEM-based jellyfish robot. When the CFEM-based jellyfish robot dives toward the water surface, the 3D deformation decreases and the conductive path is recovered, resulting in decreased resistance (Figure 5f). Note that electrical signals can identify the directionality of motion patterns, making important prospects for monitoring the underwater motions of creatures.

To mimic the warning behavior of natural jellyfish, we developed an underwater environment interaction system. The CFEM-based jellyfish interaction system includes the ultraviolet light source, sensing (CFEM), program control (microprocessor), and driving systems (micromotor and pulleys), which can effectively simulate and achieve the function of jellyfish skin perception and autonomous color changing. The schematic diagrams and photographs of the close-loop feedback system are displayed in Figure S32. The self-supported CFEM, which is integrated into the artificial jellyfish robot, is able to sense external vibrations and/or disturbances through the water flow. Tiny water vibrations induce the membrane to stretch and produce an electrical signal (ΔR). The generated electrical signal is transmitted to the microprocessor, and the program judgment of Figure 5g is carried out. When the $\Delta \mathrm{R}$ exceeds the predetermined threshold, the system will classify the CFEM-based jellyfish as in a hazardous condition and manipulate the jellyfish robot driving toward deeper water via micromotors and pulleys. Conversely, the jellyfish robot is considered in a safe condition and does not require actions. As shown in Figure 5h, when the jellyfish robot detects a slight disturbance, such as a small fish swimming past, the normalized resistance represents a mild signal with suggestive information on safe conditions. However, when the CFEM-based jellyfish robot experiences severe mechanical stimulation, like a shark attack, it can autonomously drive and escape toward deeper water, showing an elevated normalized resistance curve. The sensing and warning process of the artificial jellyfish robot is shown in Figure 5i,j and Movies S2 and S3. It can be clearly observed that the artificial jellyfish robot maintained a consistent water depth and did not display fluorescent warning behavior while detecting a normal signal. Once the artificial jellyfish robot detected the danger signal, the micro motor controlled the jellyfish robot driving from 0 to 150 cm underwater at a constant speed of ~3.41 cm/s. During this process, the red fluorescence gradually appeared to achieve a fluorescence warning as the 3D morphing increased. The designed CFEM-based jellyfish robot and the fluorescence warning mechanism provide potential feasibility for underwater soft robots with multiple functions.

3. CONCLUSIONS

In this work, we have constructed self-perceptive and autonomic 3D deformative fluorescent soft skins and further designed an artificial jellyfish robot for close-loop control of sensing, processing, actuating, morphing, and color display in the water environment. Benefitting from the molecular-level water surface, the thin and integrated soft actuators can be rationally designed, allowing the formation of suspended membranes (decades of microscales) in an air chamber for autonomic underwater actuation. Our soft thin skin-based actuators possess some advantages over existing systems, including the highly structural integration, the autonomic 3D morphing under water conditions, synergetic sensory-actuating-color changing functions, and their feedback system. To further demonstrate the potential of the soft skins, the artificial jellyfish robot is designed to achieve underwater multicolor/gradient fluorescence visual display. Also, the robot with a closed-loop system can actively perceive external normal and even dangerous stimuli and further drive into deep water with autonomic 3D morphing and simultaneous fluorescence warning, showing significant potential in underwater visual environmental interaction systems.

4. MATERIALS AND METHODS

4.1. Materials. The raw carbon nanotubes (CNTs) (length, about 10−30 μm; diameter, about 10−30 nm; −COOH %, about 2 wt %) with a purity of over 90% were acquired from Chengdu Organic Chemistry Co., Ltd., and were rinsed thoroughly with anhydrous ethanol and dried in a stream of nitrogen before use. Silicon rubber (Ecoflex 00−50) was purchased from Smooth-on, USA. Prior to spray-coating, components A and B were mixed with a 1:1 weight ratio and consequently diluted using hexane with a weight ratio of 8.7%. Oil soluble fluorescent pigment purchased from Guangzhou Xinyan New Material Co., LTD can fluoresce brightly under a 254/365 nm ultraviolet lamp. General chemicals of chemical reagent grade were used as received from Sinopharm Chemical Reagent.

4.2. Fabrication of Assembled CNT Films. A certain amount of CNTs was well-dispersed in the ethanol solution using the ultrasonic method. The ethanol-dispersed CNT suspensions were further sprayed on the air/water interface by a spray-coating method. To achieve a homogeneous film, the location of the sprayer should be changed in an orderly manner during the spray-coating process. Subsequently, a commercially available sponge was employed to drive the preassembled film to form a condensed structure, in which the procsiphon effect induced effective water absorption. Simultaneously, CNT preassembled films were closely packed toward the opposite direction of the siphone direction followed by a prominent decrease in the preassembled CNT film area, and finally, a homogeneous CNT film was obtained. It is noted that the concentration of CNT suspension can be adjusted to 0.3, 0.5, 1.0, 1.5, and 2.0 mg/mL. The fluorescence display intensity of artificial jellyfish can be successfully modulated by the concentration of CNTs.

4.3. Fabrication of CFEM-Based Bioinspired Skins. The oil-soluble fluorescent pigment (0.03 g) was fully dissolved in the well-dissolved mixture of Ecoflex and *n*-hexane solution (30 mL) by an ultrasonic method. Then, the fluorescent elastomer solution was carefully dropped onto the surface of the as-prepared CNT film for a uniform layer. Note that in order to obtain a uniform fluorescent elastomer membrane, the well-dispersed fluorescent elastomer solution should be dropped at a constant speed along the container wall. When the *n*-hexane solvent evaporated, a typical curing procedure (25 °C for 6 h) was achieved, resulting in a robust and homogeneous CNTs-fluorescent elastomer hybrid film on the water surface.

4.4. Fabrication of the Artificial Jellyfish Robot with Self-Perception and 3D Deformation. The detailed structure of the jellyfish-like artificial robot is shown in Figure 2a. The fluorescent jellyfish robot consists of a UV LED lamp, transparent cover, electrode, fluorescent skins, and hollow base. The volume of the fluorescent jellyfish robot is determined by the diameter of the transparent cover (poly(methyl methacrylate) (PMMA)) (60 mm for a single jellyfish and 90 mm for an integrated jellyfish). First, a UV LED lamp (model: UVC3535, size: 20 mm × 20 mm, excitation wavelength: 250−260 nm, voltage: 8 V) was fixed on the top of the transparent cover by double-sided foam adhesive and welded to a separate power supply. Subsequently, the hollow base was obtained by laser cutting, and CNTs/fluorescent elastomers adhered to the center of the Hollow bases using PDMS prepolymer. Note that in order for the fluorescent skins to adhere tightly to the substrate, the surface of the hollow base should be roughened with sandpaper and further cleaned with ethanol before the skin adheres. Then the device was cured at 60 °C for 1 h, and the electrode was constructed with a silver paddle and aluminum wire. Finally, the transparent cover and the hollow base adhered CNTs/fluorescent elastomers were assembled and sealed by Ecoflex prepolymer to ensure the sensing layer without water. With the increase of water depth, the imbalance between internal air pressure and external water pressure of the artificial jellyfish robot causes three-dimensional deformation.

4.5. Abaqus Simulation Analysis of Water-Pressure-Induced 3D Strain Distribution. The finite element simulation model was built based on real experimental conditions. The deformable elastomer film with a diameter of 20 mm and thickness of 0.1 mm is integrated into a transparent hemispherical plastic cover with a diameter of 60 mm. The diameter of deformable CFEM was measured directly by vernier calipers, while the thickness was estimated from the cross-sectional SEM images. The density and Poisson's ratio of the model were calculated as 1.07 g cm $^{-3}$ and 0.49, respectively, and the elastic modulus of CFEM can be calculated as 1288 kPa from the slope of the stress−strain curve in the range of 0−496% (Figure S6). A geometric nonlinear model was used for the whole simulation. The surface of the elastic film is designed with microcracks and a uniform vertical upward distribution of forces is applied at the low end of the model. The loading force is gradually increased until the film breaks, and the three-dimensional strain distribution is calculated.

4.6. Experiments on Underwater Actuation and Warning Systems Based on CFEM Jellyfish Robot. The underwater environment interaction systems include a light source system (UV LED lamp), sensing system (CFEM), programmed control system (STM32F405 microprocessor), and driving system. The driving system consists of the self-manufactured micromotor and CFEM jellyfish robot connected by a removable rope. The jellyfish robot is driven from the top of the tank (tank height: 2 m) and executes the instructions and underwater movement via the Kalman filtering algorithm. When the jellyfish robot is subjected to external stimuli, the programmed control system collects the signals from the jellyfish robot and calculates the following action, which will be transmitted to the micromotor. Under the action of the driving system, the artificial fluorescent jellyfish deformed, owing to the imbalance between the external water pressure and the internal air pressure. With the depth of the water increased, the fluorescence of the artificial jellyfish was gradually exposed to achieve an underwater fluorescence warning.

4.7. Characterization. Field emission scanning electron microscopy (FE-SEM) images were obtained with an FE scanning electron microanalyzer (Hitachi-S4800, 4 kV). Static water contact angles were probed by using a contact angle meter (OCA25, Data Physics) with a 3 μL droplet of water as an indicator. Microscopic images of untangled multi-walled carbon nanotubes were obtained by transmission electron microscopy (TEM) (JEOL2100). The microcrack images were captured by a metallographic microscope (NMM-800RF). Steady-state fluorescence spectra were measured by a Hitachi F-4600 fluorescence spectrofluorometer with a xenon lamp (150 W). The digital photos of the fluorescent actuators were recorded by a smartphone camera (HUAWEI 30 Pro) under a UV lamp (ZF-5, 8 W, 254 nm). The microscopic images of CNTs stretching were captured with an OLYMPUS BX51 polarizing microscope. An electrochemical workstation (CH Instruments, CHI660E.Chenhua Co., Shanghai, China) was used to record the underwater real-time current (I) of the robot accompanied by a constant voltage (V_0) of 1 V, while the real-time resistance (R) was calculated by the equation $R = V_0/I$. The tensile test was conducted on the Z1 Zwick/Roell Universal Testing System.

ASSOCIATED CONTENT

Supporting Information

The Supporting Information is available free of charge at https://pubs.acs.org/doi/10.1021/acsnano.4c06714.

Flexible CEM skins with reversible fluorescence displays via strain-dependent cracks (MP4)

CFEM jellyfish robot in a safe underwater environment (MP4)

Underwater autonomous 3D deformation and fluorescence warning of CFEM jellyfish robot (MP4)

Details of structure and characterization of CFEM, regulation in time and space dimension of artificial jellyfish through diameter and concentration design, and more electrical and fluorescent warning properties of bubbling robots with automatic 3D morphable films (PDF)

AUTHOR INFORMATION

Corresponding Authors

Peng Xiao − *Key Laboratory of Advanced Marine Materials, Ningbo Institute of Materials Technology and Engineering, Chinese Academy of Sciences, Ningbo 315201, China; School of Chemical Sciences, University of Chinese Academy of Sciences, Beijing 100049, China;* orcid.org/0000-0003-2231-9824; Email: xiaopeng@nimte.ac.cn

Junjie Wei − *Key Laboratory of Advanced Marine Materials, Ningbo Institute of Materials Technology and Engineering, Chinese Academy of Sciences, Ningbo 315201, China; School of Chemical Sciences, University of Chinese Academy of Sciences, Beijing 100049, China;* orcid.org/0000-0003-3403-4308; Email: weijunjie@nimte.ac.cn

Tao Chen − *Key Laboratory of Advanced Marine Materials, Ningbo Institute of Materials Technology and Engineering, Chinese Academy of Sciences, Ningbo 315201, China; School of Chemical Sciences, University of Chinese Academy of Sciences, Beijing 100049, China;* orcid.org/0000-0001-9704-9545; Email: tao.chen@nimte.ac.cn

Authors

Shan Li − *Key Laboratory of Advanced Marine Materials, Ningbo Institute of Materials Technology and Engineering, Chinese Academy of Sciences, Ningbo 315201, China; School of Chemical Sciences, University of Chinese Academy of Sciences, Beijing 100049, China*

Qiling Wang − *Key Laboratory of Advanced Marine Materials, Ningbo Institute of Materials Technology and Engineering, Chinese Academy of Sciences, Ningbo 315201, China; School of Chemical Sciences, University of Chinese Academy of Sciences, Beijing 100049, China*

Jiang He − *CAS Center for Excellence in Nano Science, Beijing Key Laboratory of Micro-Nano Energy and Sensor, Beijing Institute of Nanoenergy and Nanosystems, Chinese Academy of Sciences, Beijing 101400, P. R. China*

Xinrui Liu − *Key Laboratory of Advanced Marine Materials, Ningbo Institute of Materials Technology and Engineering, Chinese Academy of Sciences, Ningbo 315201, China*

Yaowen Wang − *The First Affiliated Hospital of Ningbo University, Ningbo 315020, China*

Complete contact information is available at: https://pubs.acs.org/10.1021/acsnano.4c06714

Author Contributions

S.L. and P.X. conceived the idea. S.L. designed the experiments and performed the material preparation and characterization. S.L. performed the modeling and the work of underwater fluorescence warning with the help of Q.W. and X.L. J.H. and Y.W. helped with writing and theoretical calculations. T.C., J.W., and P.X. supervised the project. T.C. and P.X. provided financial support. All the authors provided discussion and comments.

Notes

The authors declare no competing financial interest.

ACKNOWLEDGMENTS

This project was financially supported by the National Key Research and Development Program of China (2022YFC2805200), the Natural Science Foundation of China (52373094, 52073295), the Youth Innovation Promotion Association of Chinese Academy of Sciences (No.2023313), Sino-German Mobility Program (M-0424), Ningbo Major Research and Development Plan Project (20241ZDYF020148), and Ningbo International Cooperation (2023H019). The authors also thank Prof. Patrick Théato from the Karlsruhe Institute of Technology for his thoughtful suggestions.

REFERENCES

(1) Guo, Q.; Huang, B.; Lu, C.; Zhou, T.; Su, G.; Jia, L.; Zhang, X. A cephalopod-inspired mechanoluminescence material with skin-like self-healing and sensing properties. *Mater. Horiz.* **2019**, *6* (5), 996−1004.

(2) Barbosa, A.; Allen, J. J.; Mathger, L. M.; Hanlon, R. T. Cuttlefish use visual cues to determine arm postures for camouflage. *Proc. Biol. Sci.* **2012**, *279* (1726), 84−90.

(3) Hanlon, R. T.; Chiao, C. C.; Mathger, L. M.; Barbosa, A.; Buresch, K. C.; Chubb, C. Cephalopod dynamic camouflage: bridging the continuum between background matching and disruptive coloration. *Philos. Trans R Soc. Lond B Biol. Sci.* **2009**, *364* (1516), 429−437.

(4) Hanlon, R. Cephalopod dynamic camouflage. *Curr. Biol.* **2007**, *17* (11), R400−404.

(5) Teyssier, J.; Saenko, S. V.; van der Marel, D.; Milinkovitch, M. C. Photonic crystals cause active colour change in chameleons. *Nat. Commun.* **2015**, *6* (1), 6368.

(6) Morin, S. A.; Shepherd, R. F.; Kwok, S. W.; Stokes, A. A.; Nemiroski, A.; Whitesides, G. M. Camouflage and Display for Soft Machines. *Science* **2012**, *337* (6096), 828−832.

(7) Widder, E. A. Bioluminescence in the Ocean: Origins of Biological, Chemical, and Ecological Diversity. *Science* **2010**, *328* (5979), 704−708.

(8) Polygerinos, P.; Correll, N.; Morin, S. A.; Mosadegh, B.; Onal, C. D.; Petersen, K.; Cianchetti, M.; Tolley, M. T.; Shepherd, R. F. Soft Robotics: Review of Fluid-Driven Intrinsically Soft Devices; Manufacturing, Sensing, Control, and Applications in Human-Robot Interaction: Review of Fluid-Driven Intrinsically Soft Robots. *Adv. Eng. Mater.* **2017**, *5*, No. e201700016.

(9) Kim, S.; Laschi, C.; Trimmer, B. Soft robotics: a bioinspired evolution in robotics. *Trends Biotechnol.* **2013**, *31* (5), 287−294.

(10) Barbosa, A.; Allen, J. J.; Mäthger, L. M.; Hanlon, R. T. Cuttlefish use visual cues to determine arm postures for camouflage. *Proc. R. Soc. B* **2012**, *279* (1726), 84−90.

(11) Widder, E. A. Bioluminescence in the ocean: origins of biological, chemical, and ecological diversity. *Science* **2010**, *328* (5979), 704−708.

(12) Hastings, J. W. Biological diversity, chemical mechanisms, and the evolutionary origins of bioluminescent systems. *J. Mol. Evol.* **1983**, *19* (5), 309−321.

(13) Wang, T.; Joo, H.-J.; Song, S.; Hu, W.; Keplinger, C.; Sitti, M. A versatile jellyfish-like robotic platform for effective underwater propulsion and manipulation. *Sci. Adv.* **2023**, *9* (15), No. eadg0292.

(14) Wang, Y.; Zhang, P.; Huang, H.; Zhu, J. Bio-Inspired Transparent Soft Jellyfish Robot. *Soft Robot.* **2023**, *10* (3), 590−600.

(15) Mu, J.; Wang, G.; Yan, H.; Li, H.; Wang, X.; Gao, E.; Hou, C.; Pham, A. T. C.; Wu, L.; Zhang, Q.; et al. Molecular-channel driven actuator with considerations for multiple configurations and color switching. *Nat. Commun.* **2018**, *9* (1), 590.

(16) Larson, C.; Peele, B.; Li, S.; Robinson, S.; Totaro, M.; Beccai, L.; Mazzolai, B.; Shepherd, R. Highly stretchable electroluminescent skin for optical signaling and tactile sensing. *Science* **2016**, *351* (6277), 1071−1074.

(17) Rus, D.; Tolley, M. T. Design, fabrication and control of soft robots. *Nature* **2015**, *521* (7553), 467−475.

(18) Wu, C.; Zeng, S.; Wang, Z.; Wang, F.; Zhou, H.; Zhang, J.; Ci, Z.; Sun, L. Efficient Mechanoluminescent Elastomers for Dual-Responsive Anticounterfeiting Device and Stretching/Strain Sensor with Multimode Sensibility. *Adv. Funct. Mater.* **2018**, *28* (34), No. 1803168.

(19) Qian, X.; Cai, Z.; Su, M.; Li, F.; Fang, W.; Li, Y.; Zhou, X.; Li, Q.; Feng, X.; Li, W.; Hu, X.; Wang, X.; Pan, C.; Song, Y.; et al. Printable Skin-Driven Mechanoluminescence Devices via Nanodoped Matrix Modification. *Adv. Mater.* **2018**, *30* (25), No. e1800291.

(20) Kreit, E.; Mathger, L. M.; Hanlon, R. T.; Dennis, P. B.; Naik, R. R.; Forsythe, E.; Heikenfeld, J. Biological versus electronic adaptive coloration: how can one inform the other? *J. R Soc. Interface* **2013**, *10* (78), 20120601.

(21) Rogers, J. A.; Someya, T.; Huang, Y. Materials and Mechanics for Stretchable Electronics. *Science* **2010**, *327* (5973), 1603−1607.

(22) Spenko, M. J.; Haynes, G. C.; Saunders, J. A.; Cutkosky, M. R.; Rizzi, A. A.; Full, R. J.; Koditschek, D. E. Biologically inspired climbing with a hexapedal robot. *J. Field Robot* **2008**, *25* (4−5), 223−242.

(23) He, J.; Zhou, R.; Zhang, Y.; Gao, W.; Chen, T.; Mai, W.; Pan, C. Strain-Insensitive Self-Powered Tactile Sensor Arrays Based on Intrinsically Stretchable and Patternable Ultrathin Conformal Wrinkled Graphene-Elastomer Composite. *Adv. Funct. Mater.* **2022**, *32* (10), No. 2107281.

(24) Liang, Y.; Xiao, P.; Ni, F.; Zhang, L.; Zhang, T.; Wang, S.; Zhou, W.; Lu, W.; Kuo, S.-W.; Chen, T. Biomimetic underwater self-perceptive actuating soft system based on highly compliant, morphable and conductive sandwiched thin films. *Nano Energy* **2021**, *81*, No. 105617.

(25) Acome, E.; Mitchell, S. K.; Morrissey, T. G.; Emmett, M. B.; Benjamin, C.; King, M.; Radakovitz, M.; Keplinger, C. Hydraulically amplified self-healing electrostatic actuators with muscle-like performance. *Science* **2018**, *359* (6371), 61−65.

(26) Pikul, J. H.; Li, S.; Bai, H.; Hanlon, R. T.; Cohen, I.; Shepherd, R. F. Stretchable surfaces with programmable 3D texture morphing for synthetic camouflaging skins. *Science* **2017**, *358* (6360), 210−214.

(27) Arnold, T.; Scheutz, M. The Tactile Ethics of Soft Robotics: Designing Wisely for Human−Robot Interaction. *Soft Robot* **2017**, *4* (2), 81−87.

(28) Wehner, M.; Truby, R. L.; Fitzgerald, D. J.; Mosadegh, B.; Whitesides, G. M.; Lewis, J. A.; Wood, R. J. An integrated design and fabrication strategy for entirely soft, autonomous robots. *Nature* **2016**, *536* (7617), 451−455.

(29) Justus, K. B.; Hellebrekers, T.; Lewis, D. D.; Wood, A.; Tan, C. A biosensing soft robot: Autonomous parsing of chemical signals through integrated organic and inorganic interfaces. *Sci. Robot.* **2019**, *4* (31), No. eaax0765.

(30) Shih, B.; Shah, D.; Li, J.; Thuruthel, T. G.; Park, Y.-L.; Iida, F.; Bao, Z.; Kramer-Bottiglio, R.; Tolley, M. T. Electronic skins and machine learning for intelligent soft robots. *Sci. Robot.* **2020**, *5* (41), No. eaaz9239.

(31) Shintake, J.; Cacucciolo, V.; Floreano, D.; Shea, H. Soft Robotic Grippers. *Adv. Mater.* **2018**, *30* (29), No. 1707035.

(32) Thuruthel, T. G.; Shih, B.; Laschi, C.; Tolley, M. T. Soft robot perception using embedded soft sensors and recurrent neural networks. *Sci. Robot.* **2019**, *4* (26), No. eaav1488.

(33) Yang, Y.; Wu, Y.; Li, C.; Yang, X.; Chen, W. Flexible Actuators for Soft Robotics. *Adv. Intell. Syst.* **2019**, *2* (1), No. 1900077.

(34) Zhao, H.; O'Brien, K.; Li, S.; Shepherd, R. F. Optoelectronically innervated soft prosthetic hand via stretchable optical waveguides. *Sci. Robot.* **2016**, *1* (1), No. eaai7529.

(35) Lin, G.; Si, M.; Wang, L.; Wei, S.; Lu, W.; Liu, H.; Zhang, Y.; Li, D.; Chen, T. Dual-Channel Flexible Strain Sensors Based on Mechanofluorescent and Conductive Hydrogel Laminates. *Adv. Opt. Mater.* **2022**, *10* (5), No. 2102306.

(36) Zeng, S.; Zhang, D.; Huang, W.; Wang, Z.; Freire, S. G.; Yu, X.; Smith, A. T.; Huang, E. Y.; Nguon, H.; Sun, L. Bio-inspired sensitive and reversible mechanochromisms via strain-dependent cracks and folds. *Nat. Commun.* **2016**, *7*, 11802.

(37) Liang, J.; Li, L.; Niu, X.; Yu, Z.; Pei, Q. Elastomeric polymer light-emitting devices and displays. *Nat. Photonics* **2013**, *7* (10), 817−824.

(38) Viventi, J.; Kim, D. H.; Moss, J. D.; Kim, Y. S.; Blanco, J. A.; Annetta, N.; Hicks, A.; Xiao, J.; Huang, Y.; Callans, D. J. A conformal, bio-interfaced class of silicon electronics for mapping cardiac electrophysiology. *Sci. Transl. Med.* **2010**, *2* (24), 24ra22.

(39) Yang, W.; Yamamoto, S.; Sueyoshi, K.; Inadomi, T.; Kato, R.; Miyamoto, N. Perovskite Nanosheet Hydrogels with Mechanochromic Structural Color. *Angew. Chem., Int. Ed.* **2021**, *60* (15), 8466−8471.

(40) Yu, Z.; Niu, X.; Liu, Z.; Pei, Q. Intrinsically Stretchable Polymer Light-Emitting Devices Using Carbon Nanotube-Polymer Composite Electrodes. *Adv. Mater.* **2011**, *23* (34), 3989−3994.

(41) Cheng, T.; Li, G.; Liang, Y.; Zhang, M.; Liu, B.; Wong, T.-W.; Forman, J.; Chen, M.; Wang, G.; Tao, Y.; et al. Untethered soft robotic jellyfish. *Smart Mater. Struct.* **2019**, *28* (1), No. 015019.

(42) Li, T.; Li, G.; Liang, Y.; Cheng, T.; Dai, J.; Yang, X.; Liu, B.; Zeng, Z.; Huang, Z.; Luo, Y.; Xie, T.; Yang, W.; et al. Fast-moving soft electronic fish. *Sci. Adv.* **2017**, *3* (4), No. e1602045.

(43) Herring, P. J.; Widder, E. A. Bioluminescence of deep-sea coronate medusae (Cnidaria: Scyphozoa). *Mar. Biol.* **2004**, *146* (1), 39−51.

(44) Shimomura, O.; Johnson, F. H. Chemical nature of bioluminescence systems in coelenterates. *Proc. Natl. Acad. Sci. U. S. A.* **1975**, *72* (4), 1546−1549.

(45) Xiao, P.; Liang, Y.; He, J.; Zhang, L.; Wang, S.; Gu, J.; Zhang, J.; Huang, Y.; Kuo, S. W.; Chen, T. Hydrophilic/Hydrophobic Interphase-Mediated Bubble-like Stretchable Janus Ultrathin Films toward Self-Adaptive and Pneumatic Multifunctional Electronics. *ACS Nano* **2019**, *13* (4), 4368−4378.

(46) Russell, F. S. The Vertical Distribution of Marine Macroplankton. An Observation on Diurnal Changes. *J. Mar. Biol. Assoc. U.K.* **1925**, *13* (4), 769−809.

(47) Kim, W.; Byun, J.; Kim, J.-K.; Choi, W.-Y.; Jakobsen, K.; Jakobsen, J.; Lee, D.-Y.; Cho, K.-J. Bioinspired dual-morphing stretchable origami. *Sci. Robot.* **2019**, *4* (36), No. eaay3493.

(48) Li, G.; Chen, X.; Zhou, F.; Liang, Y.; Xiao, Y.; Cao, X.; Zhang, Z.; Zhang, M.; Wu, B.; Yin, S.; et al. Self-powered soft robot in the Mariana Trench. *Nature* **2021**, *591* (7848), 66−71.

(49) Xu, X.; Yan, B. Bionic Luminescent Skin as Ultrasensitive Temperature-Acoustic Sensor for Underwater Information Perception and Transmission. *Adv. Mater.* **2024**, *36*, No. 2309328.

(50) Liu, Y.; Sun, L.; Feng, W.; Jin, Z.; Wang, C. A Stable, Self-Healable, and Stretchable Dielectric Polymer for Electroluminescent Device Working Underwater. *Adv. Funct. Mater.* **2024**, No. 2402453.

(51) Yu, C.; Li, Y.; Zhang, X.; Huang, X.; Malyarchuk, V.; Wang, S.; Shi, Y.; Gao, L.; Su, Y.; Zhang, Y.; et al. Adaptive optoelectronic camouflage systems with designs inspired by cephalopod skins. *Proc. Natl. Acad. Sci. U.S.A.* **2014**, *111*, 12998−13003.